48th AIAA Aerospace Sciences Meeting Including the New Horizons Forum and Aerospace Exposition
4 - 7 January 2010, Orlando, Florida

AIAA 2010-1112

Hypersonic Laminar-Turbulent Transition Experiment Design: From wind tunnel model definition to MDOE Approach.

A..Marino[1] and R. Fauci[2],
CIRA (Italian Aerospace Research Centre), Capua, Italy, 81043

R.Donelli[3]
CIRA (Italian Aerospace Research Centre), Capua, Italy, 81043

and

A.Schettino[4]
CIRA (Italian Aerospace Research Centre), Capua, Italy, 81043

This paper describes the Design of Experiment to study the laminar-turbulence transition phenomenon in Hypersonic regime on a 3-deg half-angle sphere-cone model. The huge number of factors (as bluntness, distributed roughness, Mach and Reynolds numbers, etc.), that affect the laminar-turbulent transition, makes this phenomenon very complex and expensive to study with a typical experimental approach.

As consequence, a Modern Design Of Experiment approach was adopted to develop highly efficient experiment designs yielding results to within a specified accuracy and, at the same time, saving resources in terms of costs and time consuming.

Preliminary numerical analyses have been performed on several sphere-cone geometries for several values of the Mach and Reynolds numbers in order to define the basic requirements for the experimental test campaign. Moreover, an innovative and simple rough nose realization methodology definition was an essential step of the experiment design phase, as it conferred to MDOE technique, the mandatory freedom in terms of number of noses and values of roughness selection.

Nomenclature

CIRA	=	Italian Aerospace Research Centre
TPS	=	thermal protection system
MDOE	=	Modern Design of Experiment
OFAT	=	One Factor At Time
k	=	Roughness height inducing transition
δ	=	Boundary layer thickness

[1] Researcher/Test Engineer, Transonic Wind Tunnel.Laboratory, a.marino@cira.it
[2] Senior Design Engineer, Test Systems Development Laboratory, r.fauci@cira.it
[3] Senior Researcher, Aerodynamics and Aeroacustics Methods Laboratory., r.donelli@cira.it.
[4] Aerothermodynamic and Combustion Laboratory.head, a.schettino@cira.it

δ^* = Displacement thickness
θ = Boundary layer momentum thickness
r = Nose Radius
$\overline{H}$ = Enthalpy
d = polynomial order
K = Number of independent variables
t_α = Type I statistical error
t_β = Type II statistical error
Re = Reynolds number
Re_{xt} = Reynolds number calculated using the transition abscissa as reference length.
Re_r = Reynolds number calculated using the nose radius as reference length.
H = Roughness Height.

I. Introduction

THE thermal protection system (TPS) of re-entry vehicles is subjected to an extremely high convective heat flux and consequently, the wall surface temperature of the vehicle increases dramatically. The thermal loads are dominated by the convective heat transfer, which mainly depends from the vehicle configuration, re-entry trajectory and heat transfer mechanisms. If a turbulent boundary layer acts on the vehicle surface, convective thermal loads can be up to 5 times higher than for laminar flow[1]. As consequence, two disadvantages can be envisaged: first an increase of the weight of a re-entry vehicle (with a consequent reduction of the payload) and second, the choice of an expensive material able to support high thermal loads. Generally the flow is transitional and it becomes important to accurately predict transition. In fact, an inaccurate estimation of the transition from laminar to turbulent boundary layer can have negative effects on the evaluation, for example, of the flap efficiency, or of the thermal loading, since the extent of the re-circulation region resulting from shock wave/boundary layer interaction (SWBLI) will dramatically change depending on the boundary layer state. In case of transitional interaction, a large heat flux peak may be observed close to the flow re-attachment location.

These are some of the reasons for which transition has long been identified as one of the critical points requiring further studies and investigations in the framework of aerothermodynamics, with the objective to develop the ability to predict and to control transition in boundary layers on re-entry vehicles. The understanding of the mechanisms leading to transition and the development of reliable transition prediction methods are recognized as critical issues in aerothermodynamics. In this work the design of a CIRA experiment, to be performed in next months, will be illustrated.

II. Aim of the Experiment

The experiment has the objective to improve the understanding of the transition mechanisms in hypersonic flow and, at the same time, to improve the effectiveness of the existing transition prediction criteria taking into account the effects of the presence on the nose of distributed roughness and of the bluntness. The idea is to perform numerical and experimental activities in order to investigate the bluntness and the distributed roughness effects on a 3-deg half-angle sphere-cone model, taking into account Reynolds and Mach number variations. Since these experiments will be performed in a conventional ground facility, the results will be compared to the Purdue Mach-6 Quiet-Flow Ludwieg Tube, in cooperation with Prof. Schneider, to estimate the effects of the wind tunnel turbulence.

In order to develop highly efficient experiment designs yielding results to within a specified accuracy, and at the same time saving resources in terms of costs and time consuming, a MDOE approach was adopted. Wind tunnel model detailed requirements definition are also an important output of this statistical methodologies.

III. Background

A. Generality

It well known, that many transition experiments were carried out in the past 50 years over conventional ground-testing facilities[2]. Extensive investigation performed in the 60's ([3],[4][5]) led to the formulation of experimental databases for the prediction of hypersonic roughness induced boundary layer transition. However, these experiments are contaminated by the high levels of noise that radiate from the turbulent boundary layers normally present in the nozzle and on the walls of the wind tunnel [6]. These noise levels, typically 0.5- 1% of the mean, are an order of

magnitude larger than those observed in flight [3][5]. These high noise levels can cause transition an order of magnitude earlier than in flight [7],[8]. In addition, the mechanisms of transition dominating in small-disturbance environments can be changed or bypassed altogether in high-noise environments; these changes in the mechanisms causes the change of the parametric trends in transition. As consequence, the transition criteria become a function of the environment in which they have been developed.

B. Bluntness Influence

The heating developing on the nose region of an hypersonic re-entry vehicle strongly depends from nose bluntness and the effects of this bluntness can be experienced by the flow hundreds of nose tip radii downstream[9],[10]. How downstream, this depends not only from the bluntness but also from the free stream conditions, as well from the smoothness refinement of the nose surface. Leading edge bluntness also influences viscous-inviscid interaction, flow separation, pressure and velocity distributions, skin friction, heat transfer, and other properties. Numerous experiments have been performed to understand the effects of the bluntness on the transition. It has been demonstrated that in presence of low noise the evolution of small disturbances in the laminar boundary layer is in a good agreement with what is predicted by the linear stability theory. The strong bow-shock generated by the bluntness of the nose produces a high specific entropy layer with strong entropy gradients that enters the boundary layer. This entropy layer interacts with the viscous layer promoting its growth. As consequence, the entropy layer promotes changes of the flow properties in the boundary layer and introduces a velocity and pressure gradient at the outer edge of the boundary layer [11][12]. The variable entropy effects caused by nose bluntness are 'swallowed' by the boundary layer at a certain length (termed the swallowing length) downstream of the nose. This, in turn, changes the properties of the boundary layer and the point at which transition occurs[13].

The bluntness effect is very complex to investigate: Generally, on cone geometries, the increases of the nose radius lead to a delay of the transition for small noses, whereas the effects become stronger and reversed for noses radii above an "optimum radius" (Fig. 1). This is known as the "bluntness paradox". Fig. 1 and Fig. 2 depict that the optimum nose radius at which the trends inverts depends on the nose radius and the Reynolds number .

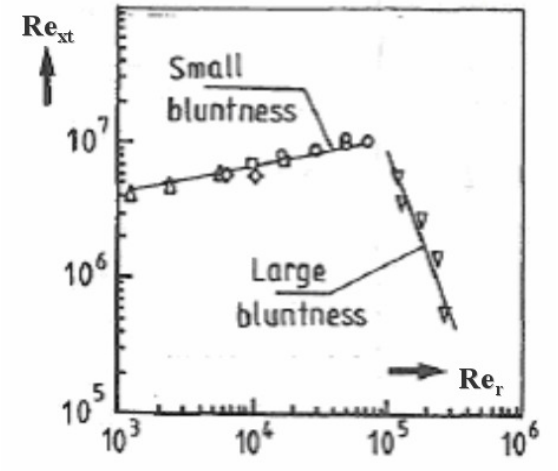

Fig. 1: Nose effects on transition location on a 3° semi angle cone model ([14])

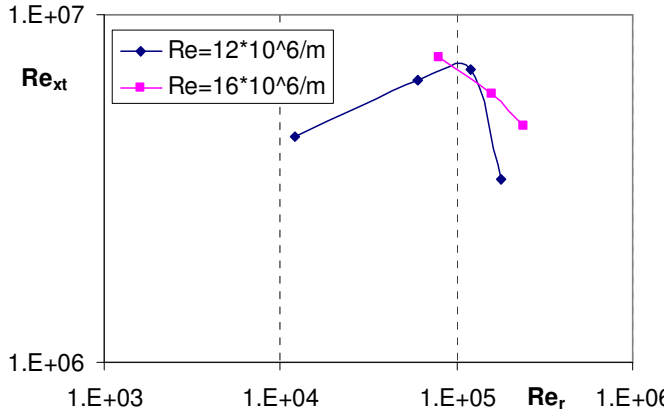

*Fig. 2: Nose effects on transition location on a 3° semi angle cone model (**.[15]**)*

C. Distributed Roughness Influence

The second aspects, of interest, are the effects on transition of the distributed roughness. The materials usually used to realize the thermal protection system are located in the nose region and the surface smoothness is slightly rough. In addition, during the flight, heat fluxes are so high that erosion phenomena can be expected. As consequence a distributed roughness can take place on the nose surface, affecting the boundary layer transition from laminar to turbulent regime. The question is: What is the range of roughness heights that has to be investigated in order to capture the roughness effect on transition?

IV. CFD Analysis and Numerical Procedure for Basic Requirement Definition

A. CFD Analysis Description

In order to optimize the experiments, it necessary to minimize the costs and maximize the efficiency. This objective can be achieved by minimizing both the number of test articles necessary to the experiment and the number of runs.

In this work the nose radius range to be investigated has been fixed on the base of the experience and with the requirement to experience the bluntness paradox, while the range of roughness heights to be investigated has been defined by performing several numerical computations on a sphere-cone geometry, characterized by a nose radius ranging from 2 mm to 30 mm, for several values of the Mach and Reynolds number. The preliminary computations have been performed on a model very similar to the one of interest (the geometry is slightly different from the CIRA model, being the cone angle equal to 2.9 degrees instead of 3) and supposed to have a smooth surface. The results were compared with the available literature data[15]. In [15] it is shown that, on this kind of geometry, transition generally needs a finite length to fully develop. Fig. 3 reports the experimental transition points at M=6 on a cone geometry for several Reynolds numbers and shows that the transition length change as the nose radius and Reynolds number is changing. However, the bluntness paradox is clearly visible on the transition onset([15]).

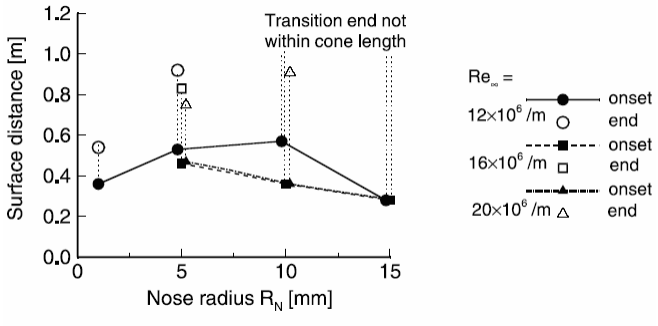

Fig. 3: Bluntness effect on transition on-set and completion; M=6[15]

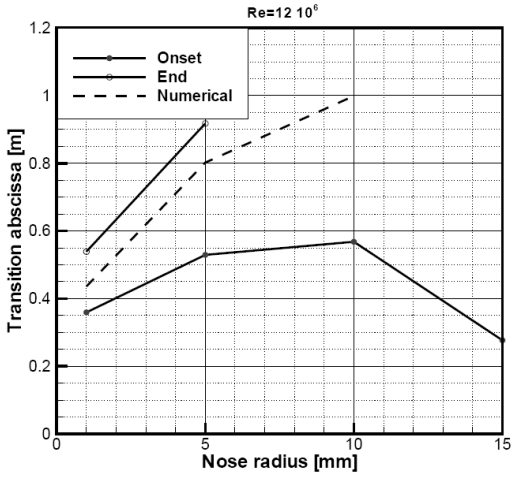

*Fig. 4: Comparison between numerical and experimenta results; M=6 – Re=12*10^6*

These tests were numerically rebuilt by means of the CIRA Navier-Stokes code H3NS, and the Anderson formula[1] was applied to the CFD solution in order to provide an estimate of the natural transition point. The comparison is shown in Fig. 4, where it can be seen that the numerically computed transition point is generally comprised in the experimentally measured transitional region. However the bluntness paradox is not predicted by the engineering formula and for a nose radius higher than 10 mm no transition is predicted along the model.

After this preliminary validation, the engineering formulas for roughness induced transition were applied to the CFD computations in order to compute the distributed roughness height able to force transition.. The objective of these investigations was to define the range of interest for the roughness to be investigated in the experimental test campaign. A post processing numerical tool developed in CIRA allows computing integral boundary quantities like displacement and boundary layer momentum thickness to be used in the engineering formulas. The application of several transition criteria like PANT, Batt & Legner, Van Driest & Blumer, Reshotko and Dirling allows computing the transition location as function of the roughness height inducing transition, here indicated with k. Here are shortly described the criteria used.

B. Criteria for Transition Prediction and Roughness Height Determination

Van Driest and Blumer criterion [16], developed for isolated spherical roughness elements placed over cones is written in a general form:

$$\mathrm{Re}_{\delta_1} = \left(\frac{k}{\delta_1}\right)^p A.B.C \qquad (1)$$

where $p \approx -1$, $\mathbf{A} = (1+\frac{\gamma-1}{2}\mathbf{M_e^2})$ is a compressibility correction, $\mathbf{B} = f(\frac{\tilde{T}}{T_e})$ a wall temperature correction, and C a pressure gradient (or curvature) factor. Various functional definitions have been used to consider multiple roughness elements and even distributed roughness. This correlation was not found accurate when compared to cone experiments[17]: Roughness heights were underestimated by a factor 2.5. More recently, a modification of this criterion was applied by NASA to Shuttle flights and wind tunnel results and was reported in 1997[18]. The modified criterion is written as

$$\mathbf{Re_{\delta_1}} = 242(1+\frac{\gamma-1}{2}\mathbf{M_e^2})\left(\frac{\mathbf{k}}{\delta_1}\frac{1}{1+\mathbf{B}/\mathbf{B_s}}\right)^{-1.1} \qquad (2)$$

where $\frac{1}{1+\mathbf{B}/\mathbf{B_s}}$ is the pressure gradient correction term, where B represents a reduced velocity gradient and B_S is the stagnation point value set to 0.5. Their results are reproduced on Fig. 5. Correlation is still not excellent: dispersion of wind tunnel data is ±65 %, and flight data (STS-28 and STS-73) are respectively +69% and +208 % from the correlation fit. Note that the NASA modification is not completely described, as the pressure gradient term is not fully defined in their presentation.

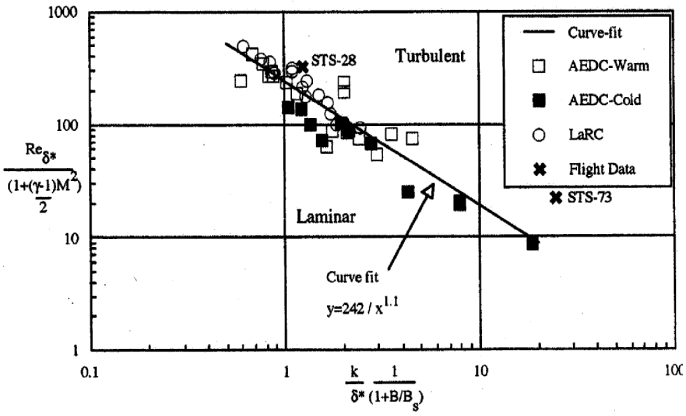

Fig. 5: NASA modified Van Driest criterion[16]

Potter and Whitfield criterion [19] is based on a Reynolds number $\mathrm{Re}_{kk} = \frac{\rho_k k U_k}{\mu_k}$, in which flow quantities are taken at the boundary layer height k corresponding to the roughness height (use of this Reynolds number seems to go back to Klebanoff in the case of low speed flows). The criterion provides an estimation of the transition movement due to roughness. It can be expressed as:

$$\left(\frac{\mathbf{x_t}}{\mathbf{x_{t_0}}}\right)^{1/2} - \frac{\boldsymbol{Re'_{kk}}}{\boldsymbol{\varepsilon}}\left(\frac{\mathbf{x_k}}{\mathbf{x_{t_0}}}\right)^{1/2} = \mathbf{f}(\frac{\boldsymbol{Re'_{kk}}}{\boldsymbol{\varepsilon}}) \qquad (3)$$

where $\mathbf{X_t}$ is the transition point in presence of the roughness, $\mathbf{X_{to}}$ the smooth wall transition point, $\mathbf{X_k}$ the roughness location. $\frac{\mathbf{R'_{kk}}}{\boldsymbol{\varepsilon}}$ is a normalized parameter $(0 \le \frac{R'_{kk}}{\varepsilon} \le 1)$ where the modified Reynolds number is defined as

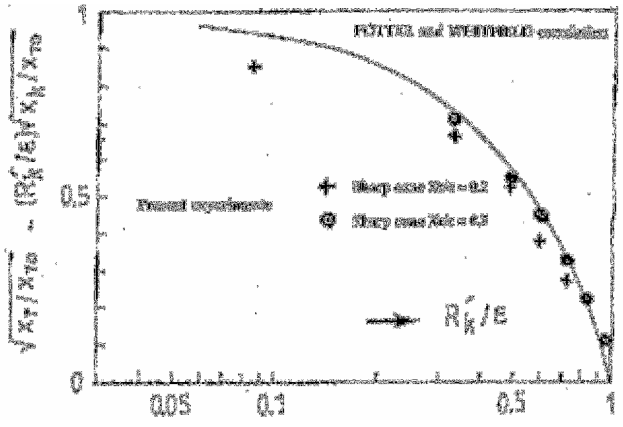

Fig. 6: Potter and Whitfield criterion [19]

$\mathbf{R'_{kk} = \frac{\rho_k k U_k}{\mu_k}\left(\frac{T_k}{T_w}\right)^{\omega+0.5}}$ and $\boldsymbol{\omega = 0.76}$ is the temperature exponent in the Sutherland viscosity law $\boldsymbol{\mu \approx T^{\omega}}$. This criterion was created based on hollow cylinder model ($\frac{dp}{dx} = 0$) experiments at Mach numbers between 3 and 5.

PANT criterion (Anderson[20]) is based on classical cold supersonic and hypersonic wind tunnel tests conducted during the 'PAssive NoseTip Program', a cold war research program dedicated to improving the design of warheads during the first half of the seventies. The semi-empirical criteria (due to Anderson, Dirling, Finson, Bishop and Van Driest) that were developed during this program were then compared to ballistic range test results conducted by Reda in 1979[21]. Anderson's criterion defines the parameter:

$$\Psi_1 = R_{\theta_c}\left(\frac{kT_e}{\theta T_w}\right)^{0.7} \quad \text{with} \quad 1 < \frac{kT_e}{\theta T_w} < 10 \tag{4}$$

and transition is then predicted where $\boldsymbol{\Psi_1 = 215}$. Since $\boldsymbol{\Psi_1}$ is generally an increasing function of x,. transition always occurs in the subsonic region, provided that $\boldsymbol{\Psi_1 \geq 255}$ on the sonic line.

Note that the PANT criteria is based on values calculated at the boundary layer outer limit ($\boldsymbol{\rho_e, U_e, T_e}$) because of the limitations at the time to determine precisely these functions at the roughness height, k, within the boundary layer, although $\mathbf{R_{kk} = \frac{k\rho_k U_k}{\mu_k}}$ was considered, at least by Reda, to be a more significant parameter: From PANT correlation

$$\mathbf{R_{\theta cT} = 215\left[\frac{kT_e}{\theta T_w}\right]^{-0.7}} \tag{5}$$

And the modified Reda' correlation is

$$\mathbf{R_{\theta cT} = 574\left[\frac{kT_e}{\theta T_w}\right]^{-1.3}} \tag{6}$$

Reda's results are reproduced in Fig. 7, showing the original correlation and his modified one:

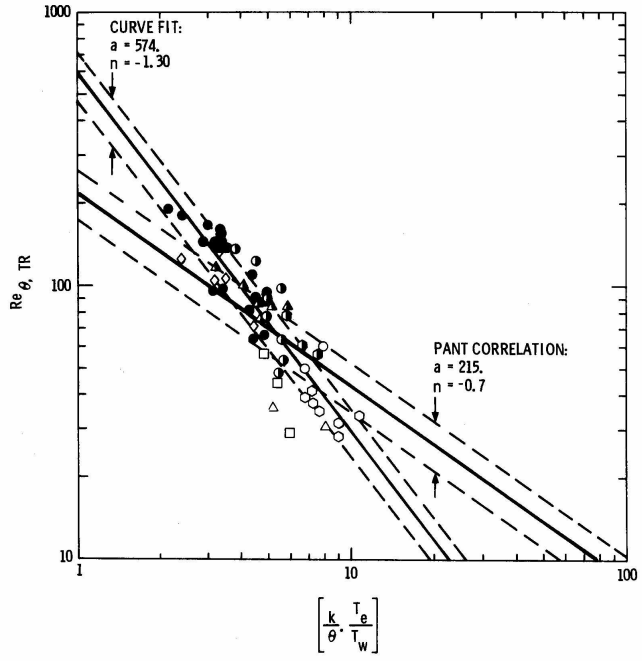

Fig. 7: Reda's results using PANT correlation [21]

BATT and LEGNER criterion[22] was defined on the PANT data and smooth wall transition data, intending to model both natural and roughness induced transitions. The parameter defined for this criterion is

$$\boldsymbol{\psi_2 = \frac{kT_e}{\theta T_w}\left(\frac{1}{1+350\frac{k}{R}}\right)} \tag{7}$$

where **R** is the nose radius. Transition is predicted when: If $\boldsymbol{\psi_2 < 1}$ $\boldsymbol{R_{\theta_{cT}} = 500}$ and if $\boldsymbol{1 < \psi_2 < 10}$ $\boldsymbol{R_{\theta_{cT}}\psi_2^{1.5} = 500}$. The first case, $\boldsymbol{\Psi_2 < 1}$, corresponds to the smooth wall. When used with the curvature correction term, the expression for **k** has two infinite branches corresponding to a zero denominator. In some cases (Space Shuttle, EXPERT geometry), this term may reasonably be neglected when transition is expected in a low curvature region.

The use of this criterion for natural transition prediction is certainly not recommended, since this local criterion does not fully take into account pressure gradients and wall temperature effects.

Recently, Reda proposed $R_{kkT} = cons\tan t$ as a universal criteria[23]. The constant being adapted depends on the configuration, on the available numerical tools and on the transition type.

Concerning to flight extrapolations, NASA[16] results reproduced on Fig. 8 show a rather large dispersion, in terms of $\mathbf{R_{kkT}}$ (values between 200 and 1000),. On the same figure, $\mathbf{R_\theta/M_e}$ varies between 60 and 200, where $\mathbf{M_e}$ is close to 2. Hence reasonable limit values for $\mathbf{R_\theta}$ on a slender reentry body should be taken somewhat below 200, closer to 120.

NASA's criteria, developed for the Space Shuttle, have also been examined. In 1981, Bertin et al [24] introduced a wind tunnel transition criteria for smooth wall Space Shuttle in a form $\mathbf{X_{Tr}/L = f(R_\theta/M_e)}$, which is an improved version of the old $\mathbf{R_\theta/M_e = 200}$ used during the fifties, then roughness effects are introduced in a correlation of $\mathbf{R_{kk}}$ with $\mathbf{R_\theta/M_e}$. In order to simplify computation, $\mathbf{R_{kk}}$ is evaluated at a single reference location $\mathbf{X/L = 0.1}$. First results are presented in Fig. 9[25]. The curve on this figure represents the smooth wall transition prediction for the Shuttle, while the dark grey region corresponds to rough wall transition predictions. Symbols correspond to several flight measurements. Moreover Fig. 9 identifies two regions: for X/L > 0.4, transition in wind tunnel is influenced by the wind tunnel noise, and appears earlier than in flight. On the contrary, for X/L<0.4, installation noise has a smaller effect and comparison to flight is in this case correct.

More recently[26], a simplified version of the **NASA criterion** was proposed as:

$$\frac{\mathbf{k}}{\boldsymbol{\delta}} = \mathbf{C}\frac{\mathbf{M}}{\mathbf{R_{\theta_C}}} \qquad (8)$$

where $\boldsymbol{\delta}$ is the physical boundary layer thickness. The constant **C** needs to be adapted, (in general **C**=35 for effective roughness height). This correlation is specific to the space shuttle geometry.. In case of other vehicles, the **C** constant has to be modified according to the geometry and to the numerical tools used for determining boundary layer parameters[27]. Re-evaluation of PANT data, combined with space Shuttle conditions, resulted in a new criterion:

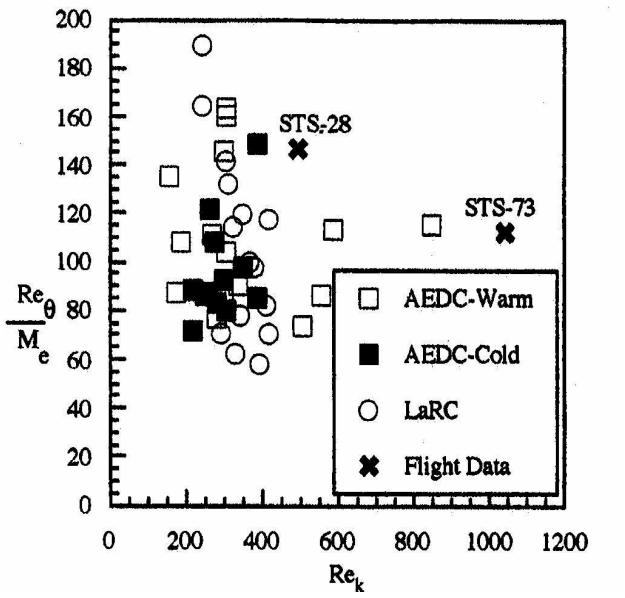

Fig. 8: Range of variations of Re_{kkT} *[16]*

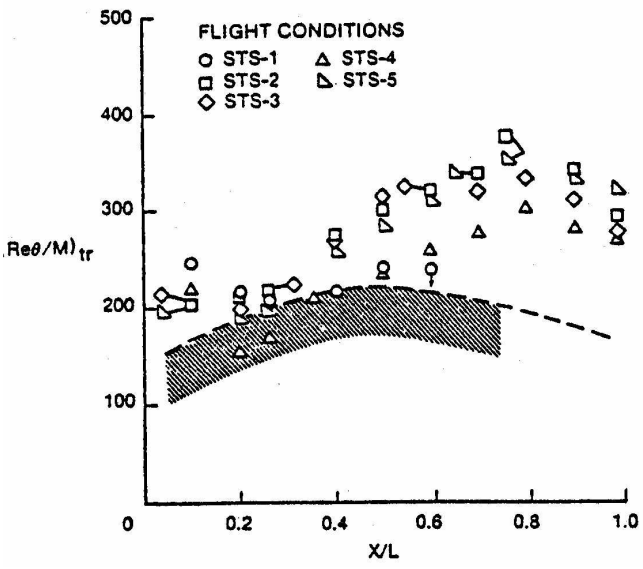

Fig. 9. Space Shuttle transition correlation (wind tunnel and flight)[25]

$$\frac{R_\theta}{M_e} = 191\left[\frac{k}{\theta}\frac{T_e}{T_w}\frac{1}{1+B/B_s}\right]^{-0.444} \qquad (9)$$

This correlation is not restricted to transition in the subsonic region. The pressure gradient correction term is again only partially defined. Comparison to wind tunnel and flight data is represented in Fig. 10[16]. Agreement to the criterion is visibly improved, compared to Figure 4 above. Dispersion from the curve is limited to roughly 50% only. Although the $\frac{1}{1+B/B_s}$ term is not fully defined, this corrective term should remain close to one in most cases, and can be neglected in many instances. From this review of transition criteria, there is no unique answer to apply to a flight vehicle. The best suggestion is to combine a number of indicators:

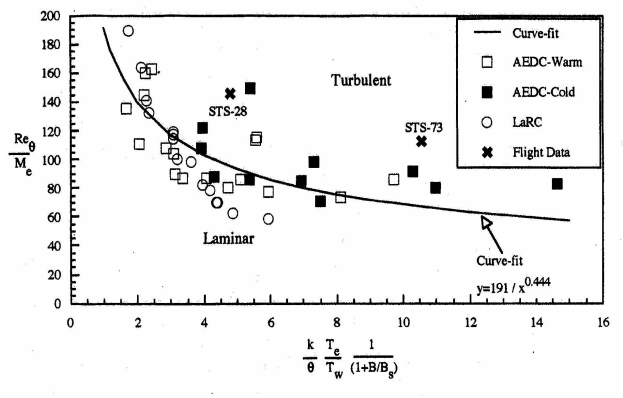

Fig. 10. NASA modified PANT criterion[16]

$$R_{kk} > 200 \quad \text{and} \quad R_\theta > 100 \quad \text{and} \quad R_{\theta cT} = 215\left[\frac{kT_e}{\theta T_w}\right]^{-0.7} \quad \text{and} \quad \frac{R_\theta}{M_e} = 191\left[\frac{k}{\theta}\frac{T_e}{T_w}\frac{1}{1+B/B_s}\right]^{-0.444} \qquad (10)$$

The nose Reynolds number Re_r, based on the nose radius, r is also a critical parameter. For $Re_r \le 10^5$, transition very close to the stagnation point, in the subsonic region, does not seem probable. For $Re_r \ge 10^6$, this type of transition, as predicted in the original PANT criterion, should be considered possible. Some authors[28] examined the effect of nose radius in case of sphere-cone models and proposed a criterion taking explicitly into account the nose Reynolds number.

C. Numerical Procedure

All the previous criteria require the knowledge of flow properties in the boundary layer, as well as the integral quantities δ^* and θ. The determination of these integral values from an Averaged Navier Stokes solution is not trivial, and attention must be paid in the choice of the criterion to identify the boundary layer thickness. Since the Navier-Stokes numerical simulation gives a continuously varying velocity from the wall to the free stream flow, the boundary layer has been rebuilt considering as definition of the boundary layer thickness the location where the local enthalpy become 0.99 of the external enthalpy ($\overline{H} = 0.99\overline{H}_e$)

This choice provides better results with respect to the classic boundary layer thickness definition because also the thermal boundary layer has been taken into account. So, δ is computed by searching the j-value related to the local normal for each discrete abscissa, where the enthalpy relation $\frac{\overline{H}_{i,j}}{\overline{H}_{i,j-1}} - 1 = 99\%$ is verified. The so founded boundary layer height distribution over the model shows strong oscillations in some points. For this reason a regression has been applied in order to obtain a continuous curve representing the boundary layer edge. Since the regression curve does not intersect the discrete points, it is necessary to interpolate all the flow properties on this curve; then the boundary layer quantities are calculated and finally the prediction criteria are applied.

D. Bluntness and distributed roughness range

As already stressed before, numerical investigations have been performed for a Mach number range from 6 up to 12, for Reynolds number range from 2.5 up to 16 millions and for a nose's radii range from 2 mm to 30 mm.

Moreover in order to evaluate the range of the distributed roughness height to be investigated, it has been decided to distribute the roughness only in the region of the nose where reasonably erosion phenomena take place during the re-entry phase of a real spatial vehicle: The roughness is supposed to be uniformly distributed on the

experimental models from the nose aft point up to a distance equal to 2 times the nose radius. Then the engineering criteria, before discussed, to estimate the roughness height, were applied to the CFD solutions.

Fig.11 and Fig. 12 show the values of the roughness height able to trig the transition at M=6 respectively for Re=2.5*10^6 and Re=12*10^6 on a cone with a 5mm nose radius. These values show that the height of the roughness needed to induce transition decreases when the asymptotic Reynolds number increases.

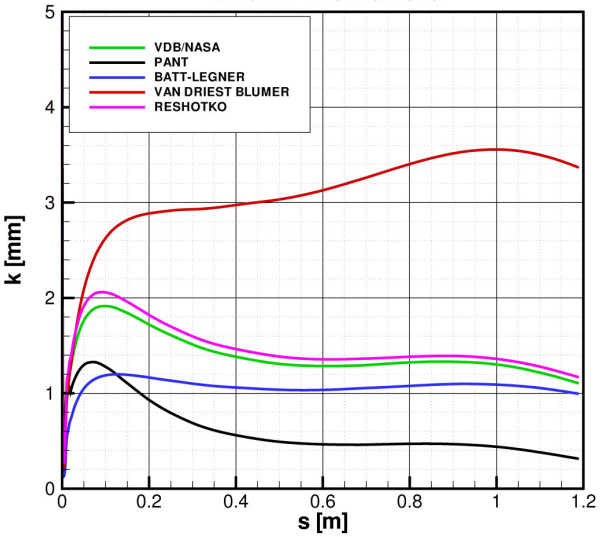

*Fig.11: Roughness height inducing transition – M=6,Re=2.5*10^6*

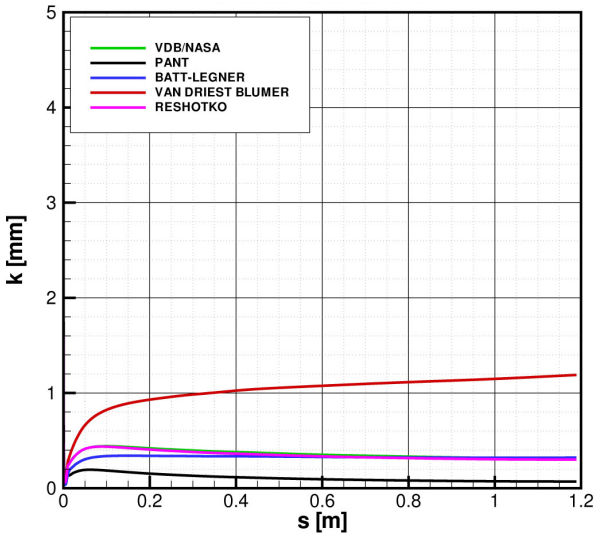

*Fig. 12: Roughness height inducing transition – M=6,Re=12*10^6*

It was experienced that PANT criterion predicts the lowest distribution of roughness heights along the surface, while Van Driest & Blumer the highest one. The distributions of k predicted by the criteria based on VDB/NASA, Batt & Legner and Reshotko tends to overlap each other, while the range of k given applying the Dirling criterion sets between these last three criteria and Van Driest & Blumer one. It can be seen that the analysis of results shows a strong discrepancy on the distribution of the effective roughness height, independently from the asymptotic Reynolds number and curvature, between the applied engineering criteria. Moreover, in some cases, applying the criteria, it has been experienced that the values of the roughness height k crosses the boundary layer height δ. Of course, it is not a realistic estimate because, obviously, an element whose dimension is higher than δ can not be further considered roughness, but a discontinuity.

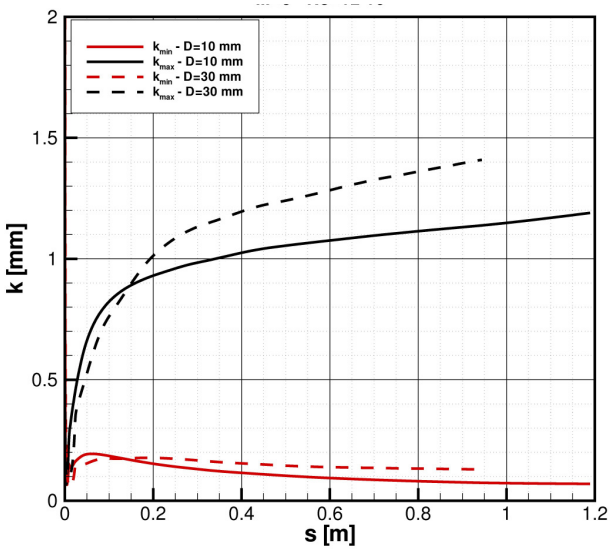

*Fig. 13: Lower and upper K values vs curvilinear abscissa – Mach 6 –Reynolds 12*10^6*

Concerning the nose radius effect, Fig. 13 shows the lower and upper K for two different diameters 10mm and 30 mm at Reynolds number of 12x10^6 and Mach=6. As can be observed, in the first region of the nose (up to 0.1 meter of the abscissa curvilinear) the effect is negligible. Finally, Fig. 14 shows the roughness limit heights at s = 0.1 m are plotted as function of the nose diameter for each criterion at M=6 and Re=12*10^6. It can be observed that for all nose radius values the PANT criterion and VDB criterion give respectively the lowest and

biggest values of k. However it must be remembered that the PANT relation is applicable only in the subsonic region close to the stagnation point, and therefore is not suitable in the considered S-station[20].

A similar study has been done to evaluate the Mach number effect on the roughness heights inducing transition. Fig. 15 shows the lower and upper K at two different Mach number values computed for the Reynolds number of $7x10^6$ and for the nose diameter of 10mm. It can be observed that the distributed roughness heights inducing transition increase in the nose region by increasing the Mach number.

In conclusion, the minimum nose radius was fixed in 5mm mainly for constructive reasons, since the heat loads could become critical in case of very sharp configurations (2 mm diameter); moreover, the bluntness range was limited to a radius of 25mm, where the bluntness effect should be predominant and the transition onset should be close to the nose. Moreover, for the nose radius of 25mm the bluntness paradox is already present for moderate low Reynolds numbers (Fig. 3).

Moreover, Since the height inducing transition strongly increase as the Mach number increases (Fig. 15), it has been decided to consider a Mach range of interest between 6 and 9.in order to limit the roughness height range to be tested experimentally.

Finally, it was experienced that the roughness height inducing transition strongly change depending on the criteria used. Since the phenomena erosion are expected to take place on the nose region in order to be sure to trigger transition it has been decided to consider in the experiments a range of k between 0 (smooth) and 1.25 mm, uniformly distributed from the nose aft point up to a distance equal to 2 time the nose radius.

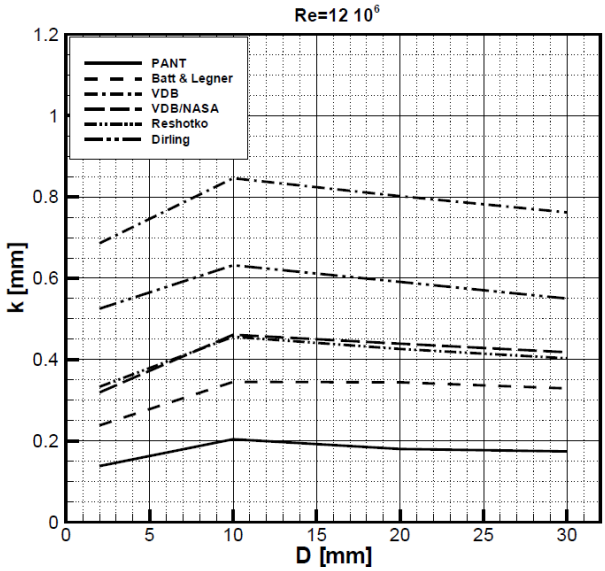

*Fig. 14: Roughness height inducing transition Vs D – at s=0.1m M=6,Re=12*10^6*

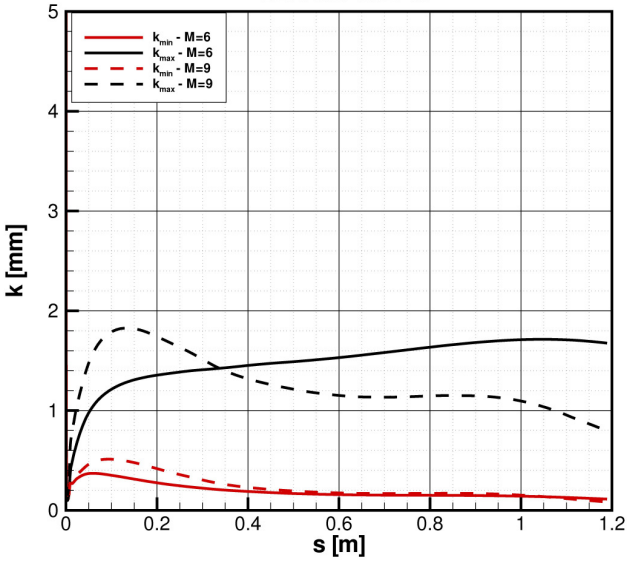

*Fig. 15: Lower and upper K values (M=6 and 9) vs curvilinear abscissa – D=10mm – Reynolds 7.0*10^6*

V. Design Of Experiments

A. MDOE Tecnique

1 Generalities

The Modern Design of experiments (MDOE) is a formal method of empirical investigation first introduced at Langley research Center in 1997 to enhance quality and productivity in large-scale, high cost experiments, and initially used for wind tunnel tests [30].

A Modern Design Of Experiment provides a means to develop highly efficient experiment designs yielding results to within a specified precision, with a typical resource saving a factor of two or more with respect to a complete OFAT design.

The One Factor At a Time (OFAT) design consist in the traditional approach to testing, that is, to vary one factor at a time, holding constant all other factors as constant. A first disadvantage of such a kind of design is the number of tests required, definitely the highest among the different existing design approach. This is generally reduced,

limiting the survey of the factors effects, along to preferential direction where the factors effects are believed to have more influence on the response variable. This is generally based simply on the researcher experience.

A modern Design Of Experiment approach allows to avoid all the main problems of the OFAT approach just mentioned above: by operating with a random selection of the tests execution, any errors from "variations in the system" during the test campaign can be overcome.

The objective of the experiment, designed with a MDOE approach, is to acquire a sufficient number of data to create one or more response surface models that can be used to predict the inducing transition phenomena, to within a specified uncertainty as a function of the main factor of interest (Re, roughness height, nose radius, etc) in the variable selected ranges. In this section the wing tunnel tests matrix definition by using the MDOE approach will be discussed in detail.

2 Establishing The Design Space

First of all the ranges of the independent variables, or the design space, must be identified. This choice can influence the number of test points and their location. For example over a narrow range for a given factor the response variable may exhibit a low-order trend, whereas over a wider range of that factor, the response may be highly non-linear, requiring many more points in order to fit an adequate response surface. As will be pointed out later, the shape of the design space has an effect as well. Many well-established experiment designs (central composite design, box-benken design etc..) with desirable properties exist for spherical or cubical design space. Irregular design space generally requires computer programs to construct an optimal design. There are several popular design optimality criteria. Perhaps the most widely used is the D-optimal criterion. A D-optimal design is one that provides the best balance of minimizing the prediction variance and minimizing the covariance between terms in the response model. [31]

Steat-Ease software package has been used to correctly define the D-optimal test points.

3 Model Choice

The data acquired during the tests will be used to fit a polynomial regression model, the response surface that describes the response variable, the transition length, as function of the factors of interest. The number of data necessary to correctly fit the regression model depends on the order of the polynomial function selected; the number of terms p in a d^{th}-order polynomial of K independent variables is given as:

$$N = \frac{(d+K)!}{d!K!} \tag{11}$$

Where N represents also the minimum number of data required to fit such a kind of model. Note that the number of data required grows rapidly as the order of the model or the number of variables increases. Thus, it is important to understand the expected functionality of the response so that the adequate response model can be described; at this scope previous result found in the literature gave insight into the behavior of the transition length.

4 Mach Number

As said in the previous sections, the Mach number is certainly an important parameter on the transition position. Unfortunately, during an experimental activity, a Mach number modification generally needs long time wind tunnel operations to modify the nozzle-test section geometry. Then, it should be more convenient (in term of cost and time) to perform consecutively all tests at the same Mach number. But, as said above, this is not compatible with the philosophy of the MDOE approach which operate with a random selection of the tests execution and a wind tunnel configuration change should be necessary after each run. For this reason. it was decided to define two model design: the first for M=6 and the second for M=9.

Finally, only few tests will be performed at Mach 12 to detect the Mach number effect on the nose-roughness geometry.

5 Reynolds effects

It has been experimentally observed [14] that an increase in the unit Reynolds number leads to an increase in the transition Reynolds number described by a law of the type:

$$\mathrm{Re}_{xt} \propto \mathrm{Re}^{l} \tag{12}$$

where l is an empirical constant that lies roughly between 0.1 and 0.6. Fig. 16 presents a typical experimental result ([14]) obtained on sharp cones. Nevertheless for the purpose of the model selection, it is assumed valid equation 12. Moreover, as can be seen in Fig. 16, the relation between $Log_{10}(\mathrm{Re}_{xt})$ and $Log_{10}(\mathrm{Re})$ is linear. Then, using a variable change, a conservative choice of a second order dependence of the transition Reynolds number from the free stream Reynolds number in the response surface is done.

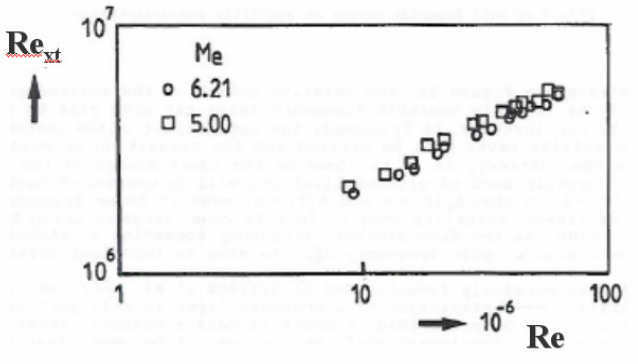

Fig. 16: Re effects on transition location on sharp cone models ([14])

6 Blunt effects

As said in B, on cone geometries, the increases of the nose radius lead to a delay of the transition for small noses, whereas the effects become stronger and reversed for noses radii above an "optimum radius" . Fig. 1 and Fig. 2 ([15]) depict that the "optimum nose radius" at which the trends inverts depends on the Reynolds number and suggests that in the response model a coupling term between the Reynolds number and the nose radius must be expected.

Also in this case an advantageous selection/transformation of the variables used to describe the phenomenon can lead to simplification of the model: the logarithm of Re_{xt} as response variable and the logarithm of Re_r as factor rather than use simply "xt" as response variable and the nose radius (mm) as factor, it results in a linear relation between two parameters in the ranges before and after the paradox.

Nevertheless, the problem to select the model to be used is now more difficult because of the strong non-linearity near the optimum radius ropt, that is difficult to model properly with a second order model. So, the best compromise is to try to fit the response surface with an high order polynomial (3rd order) in within the whole range of interest for this variable.

7 Roughness effects

Despite it can be expected that the roughness anticipate the transition, this effect is not so amply described in literature and a well known law between the roughness height and transition position is not available.

It can be hypothesized that the effect of roughness on the transition depends on the boundary layer thickness, or in other words, the transition is mainly influenced by the ratio between the boundary layer thickness and the roughness height, rather than by the latter only.

The boundary layer thickness in an hypersonic regime grows essentially as ([14]):

$$\delta \propto \frac{M_\infty^2}{\sqrt{\mathrm{Re}_x}} \tag{13}$$

Then at a fixed Mach number:

$$\frac{H}{\delta} \propto H\sqrt{\mathrm{Re}} \tag{14}$$

So, it is proposed to use the parameter $H\sqrt{\mathrm{Re}}$ as factor and the logarithm of Re_{xt} as response variable. This choice of variables should simplify the model, and then a second order dependency could be used in absence of other information on this topic.

8 Angle of Attack

It can be expected that the angle of Attack anticipate the transition position, but a law between the angle of attack and transition position is not available in literature. So, similarly to previous parameters it is decided to study the angle of attack as factor of the logarithm of Re_{xt}. This choice should simplify the model, and then a second order dependency could be used.

9 Data Volume Requirements

Eq.1 shows how a d^{th} order polynomial model in k independent variables has p coefficients and then p degree of freedom is required in order to determine these coefficients.

However, acquiring only p points would force the response surface through each point and leave no additional degrees of freedom to assess the quality of the model. By obtaining more than the minimum p points, the "floating" of the response surface it is allowed. The quality of the fit can be estimated by examining the residuals.

The total number of points necessary to construct a d^{th}-order model in k independent variables that predicts the response within a specified tolerance is given as ([30] and [32]):

$$N = \frac{(d+k)!}{d!k!}(t_\alpha + t_\beta)\frac{\sigma^2}{\lambda^2} \tag{15}$$

Here, σ is the standard deviation in the measurement, λ is the precision requirement for the response surface, and t_α and t_β are statistics related to acceptable inference error probabilities for Type I and Type II errors, respectively.

A Type I error occurs when we infer a difference between two results, say, when none exists, or when we include a response model term erroneously. A Type II error is failing to observe a true difference, or rejecting a response model term that truly exists.

From eq 15, we observe that the number of points, N, grows as the variance in the data increases, as the response model precision requirement increases as the t-statistics become larger with less tolerance for inference error. As will be seen, there is always a trade-off between the desire for high precision and the limitations in resources.

Assuming a two order model for the variable Angle of Attack, Roughness height, and Reynolds number, a third order for bluntness effect (p=19 terms), and requiring the prediction uncertainty λ to be at least equal to two time the measurement standard deviation σ ($2\sigma=\lambda$), and finally assuming 5% inference error probabilities (95% confidence levels) for both error types, the total data volume number given by Eq. 15 is N=48 test points.

At this point some considerations could be done concerning the choice of splitting the analysis in two model design (for Mach =6 and Mach=9): This implies that the total number of tests will be 96. At the contrary, considering the Mach number as a parameter (as example a two order model variable) of a unique design space the

total number of tests would be about 85. Then, concerning the total test number, this solution caused only a small difference in terms of the total number of tests, that, as said before, is largely compensated by a more rapid test execution. In stead, the more negative aspect is that this solution gives less informations in terms of interaction effects between the Mach number and the other variables on the transition location with respect to a global design. These informations will be in part recognized with dedicated tests to be performed at only few points of interest not considered in this paper.

Factor	Min	Max	Transformed Factor used in the design	Coded Name
Mach number M [-]	6	6	M	M
Angle of attack, □ [deg]	0	5	α	A
Distribute roughness height H [mm]	10^{-6} (smooth)	1.25	$H\sqrt{\mathrm{Re}}$	B
Nose Radius, r [mm]	5	25	$Log_{10}\mathrm{Re}_r$	C
Reynolds number, Re [1/m]	$2.5*10^6$	$12*10^6$	$Log_{10}\mathrm{Re}$	D

Table 1: Factors used for the design of the response surface at M=6.

Finally, another parameter to be considered to correctly define the test matrix is the leverage. The leverage is the ability of a given design point to influence the model response. High leverage points should be avoided since they unduly influence the response model and make it sensitive to outliers points in the data. In general, no one design point should have a leverage value greater than twice the average over all the points in the design space. An high leverage can be reduced by simply replicating the test points [30], [31] and [32].

B. Test Points Definition for Transition Analysis

In typical experiments design, points are chosen to allow the response model to have certain properties, such as a minimum overall prediction variance, uniform distribution of the variance over the design space, low correlation between model terms, estimation of pure error in the experiment and orthogonal blocking. The distribution of the

points in the design space determines these properties but not all the factors combinations are possible. In Table 1 and Table 2 is reported the range of interest for the considered independent variables.

As said, an "had hoc" change of variables is used to simplify the response model: r, H, Re, and Re_{xt} is substituted by the transformed variables indicated in Table 1. In the following, these transformed factors are named respectively Nose*, Roughness*, Reynolds*.

Moreover, a constrain is defined for the Nose-Roughness envelope: in fact the range of roughness heights is up to 1.25mm and this is incompatible with the minimum nose radii of 5mm. To avoid these combinations the following constrain was used:

$$\frac{r}{H} \geq 20 \qquad (16)$$

That imposes that the nose radii must be at least twenty times higher than roughness height.

Unfortunately, it is more complicated to find the equation of the constrain in the space of the transformed variables. As can be seen in Fig. 17 at each Reynolds number the equation 16 assumes a different position in the space of the transformed factors. The envelope of these curves (black straight lines in Fig. 17) should be selected as constrain, but in order to express the constrain as an inequality in the simplest way, the dashed blue and red lines are selected as constrains respectively for M=0.6 and M=0.9.

Factor	Min	Max	Transformed Factor used in the design	Coded Name
Mach number M [-]	9	9	M	M
Angle of attack, □ [deg]	0	5	α	A
Distribute roughness height H [mm]	10^{-6} (smooth)	1.25	$H\sqrt{\mathrm{Re}}$	B
Nose Radius, r [mm]	5	25	$Log_{10}\,\mathrm{Re}_r$	C
Reynolds number, Re [1/m]	2.5·*10^6	7·*10^6	$Log_{10}\,\mathrm{Re}$	D

Table 2: Factors used for the design of the response surface at M=9.

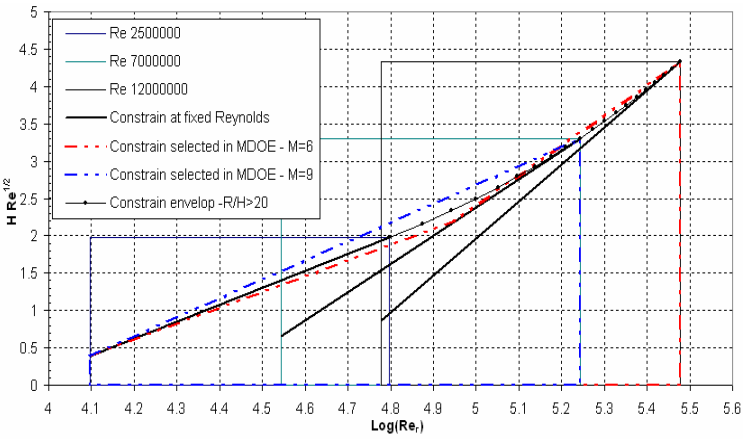

Fig. 17: Nose-Roughness* envelope and constraints*

A custom design was generated, using optimal design theory to generate what is known as D-optimal design. A D-optimal design, with 48 test point, is defined for each one Mach number of interest (M=0.6 and M=0.9) .

Clearly during the execution of the tests, it is not possible to reproduce exactly the value of the actual factors indicated in the optimal design: it should be difficult to reproduce exactly a Reynolds. This is not a problem: little shifts of the experimental points with respect to the design points don't alter considerably the quality of the design or the results. For this reason we decided to round off the values of the actual factors in order to have more realistic and easy to made values and also to reduce as much as possible the number of nose radius-roughness configurations (each one

corresponding to a different nose to be realized). The positions of the design points into the design space are plotted in figures Fig. 18,Fig. 19 and Fig. 20.

The distribution of the points appears "disorderly", but this distribution yields the lowest prediction variance. A problem that can be noted concerns the high number of nose radii-roughness combination necessary to fit the required surface model Fig. 21 shows the nose radii-roughness combinations expressed in untransformed variable necessary to cover the necessary test matrix.

The selected nose radius combinations, and the related main characteristics, are reported in Table 3

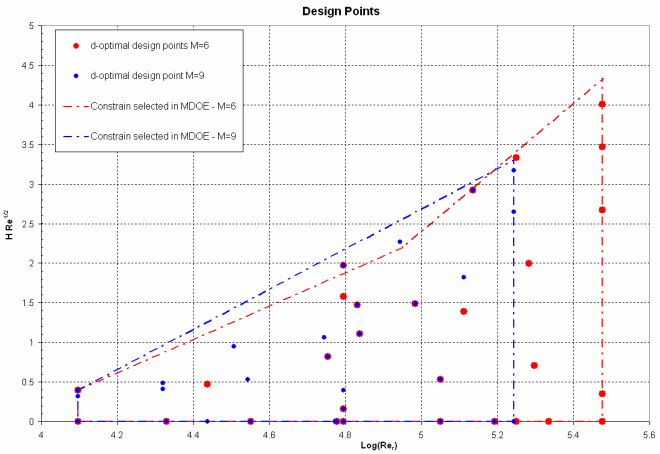

Fig. 18:D-Optimal design points in the design space Nose-Roughness**

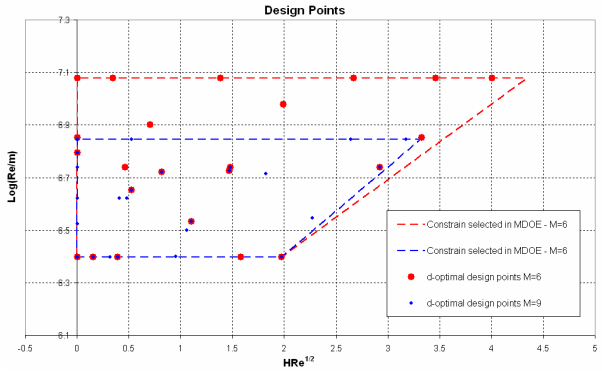

Fig. 19: D-Optimal design points in the design space Roughness-Reynolds**

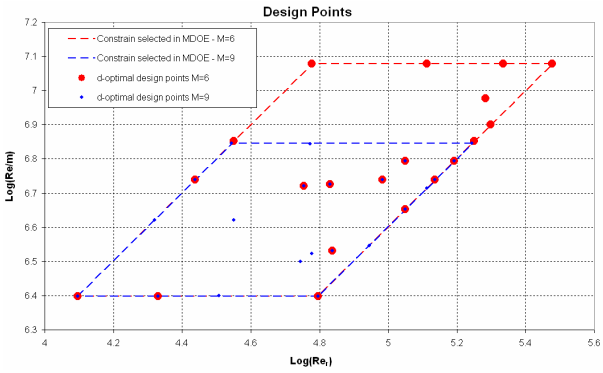

Fig. 20: D-Optimal design points in the design space Nose-Reynolds**

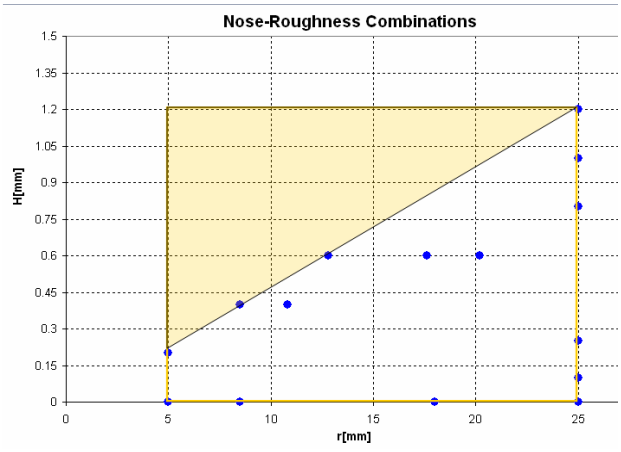

Fig. 21: Nose-Roughness Combinations

ID #	Nose [mm]	Roughness RMS [mm]
1	5.00	smooth
2	5.00	0.20
3	8.50	smooth
4	8.50	0.40
5	10.80	0.40
6	12.80	0.60
7	17.60	0.60
8	18.00	smooth
9	20.20	0.60
10	25.00	smooth
11	25.00	0.10
12	25.00	0.25
13	25.00	0.80
14	25.00	1.00
15	25.00	1.20

Table 3– Interchangeable Noses Characteristics

The quality of the design is evaluated analyzing the scaled prediction variance (also known as the standard error). As example for the experiment at M=6 (Fig. 22 and Fig. 23), it results quite low and flat within the design space.

Finally, the leverage of each point is reported in Fig. 24.

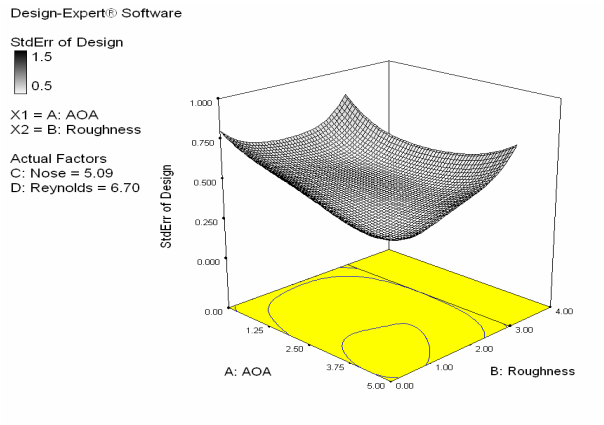

Fig. 22: Scaled prediction variance of the design at M=6 in the AOA-Roughness space*

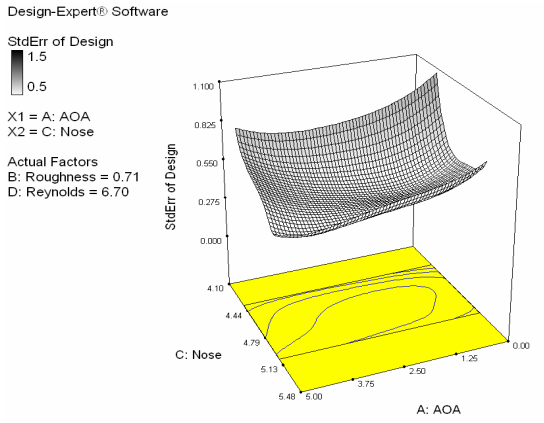

Fig. 23: Scaled prediction variance of the design at M=6 in the AOA-Nose space*

C. Confirmation Points

A well-designed experiment intended to produce a usable response surface model generally include multiple degrees of freedom to assess not only the pure error in the experiment but lack of fit in the response model as well. So after all the analysis has been performed, the quality of the response model and its ability to reliably predict the response should be investigated.

Confirmation usually involves running the experiment at off-design locations in the design space and comparing the measured data with the output of the response model at those locations. The number of confirmation points to be used is a choice based on available resources (time and cost), response model complexity, and the criticality of use of the response model. Each measured confirmation point has some degree of experimental error, so a failed confirmation trial does not necessarily reflect on the quality of the model. It is entirely possible for some of the confirmation points to lie outside of the prediction interval due to imperfections in the confirmation data rather than the model. Since a confirmation trial either "passes" or "fails" – a binary solution – confirmation success can be said to follow a binomial probability distribution. As such, the cumulative binomial probability distribution determines the number of successes that can be expected out of a total number of trials, given a probability of success of each trial and the Type I inference risk error probability for the experiment. This number of expected successes is known as the critical binomial number and is used as an objective criterion for determining whether or not a response model is valid. If the number of successful confirmation trials is greater than or equal to the critical binomial number, than the response model is said to be valid – otherwise it is not.

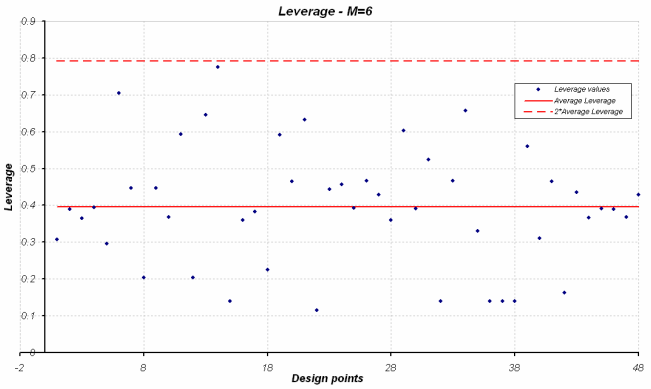

Fig. 24: Leverage of the design at M=6

For the present test campaign, we chose to use 10 confirmation points (for each one response surface) to gauge the adequacy of the response model. Given the 10% Type I error probability and a 90% probability of success of an individual confirmation trial, the critical binomial number is 7. So if at least 7 of the 10 confirmation points lie within the prediction interval, this test suggests that the model is a good one.

The confirmation points were selected such as no additional noses were needed.

VI. Wind Tunnel Model Definition

A. Wind tunnel Model description

A dedicated wind tunnel model has been designed in order to match the experiment requirements. The model has a 3° semi-vertex angle γ, a base diameter of 135mm and, as described, is equipped with several interchangeable noses, each one characterized by different radius and/or surface "roughness".

Considering that the noses radius can vary between 5mm and 25mm, the total length of the model will vary itself, depending on the nose radius adopted for the selected test configuration. The maximum model length will be of about 1150mm.

In order to fit the instrumentation and test requirements, the model will be composed of several steel parts:

- an instrumented main body and the related main body removable covering panel;
- an instrumented "main body extension" and the related extension removable covering panel;
- a set of interchangeable noses and the related "cone shaped" connection interfaces.

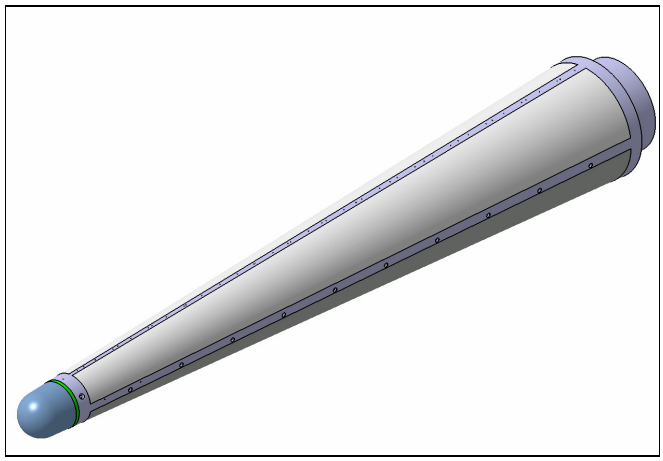

Fig. 25: Main body and nose with radius of 25mm

The main body is representative of the longest instrumented model portion allowing the installation of the nose having a radius of 25mm (see Fig. 25).

Considering that the expected location of boundary layer transition depends on the different nose radius and roughness, the instrumented extension length has been defined in order to assure the presence of the required instrumentation on the forward portion of the model when the smaller noses are installed (see Fig. 26). During the wind tunnel tests, the temperature distribution on the model surface will be acquired using infrared thermography; therefore, both, the main body and the extension will be covered with a thin layer of PeeK, a thermally insulating material. The insulating coating has been applied on the model top surface bounded by the two generatrices at j=90° j=-90°. The thickness of the insulating layer applied on the main body is 5mm. A thickness of 2mm has been adopted on the extension in order to extend as much as possible the coated portion of this model part.

The model will also be widely instrumented with pressure taps flush mounted high frequency pressure transducers, and coaxial thermocouple, in order to compare the infrared thermography results with different measuring methodologies for a correct laminar-turbulent transition point evaluation.

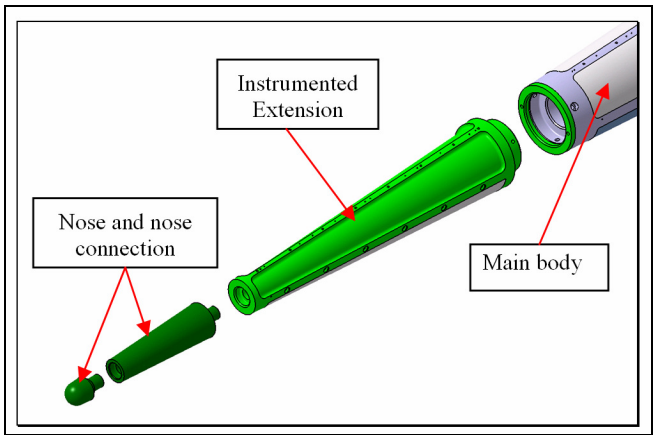

Fig. 26: Typical model assembly for nose with a smaller radius

B. An innovative methodology for rough nose realization

An innovative and at the same time simple rough nose realization methodology definition has been an essential step of the experiment design phase, in order to guarantee the necessary "degree of freedom" for the choices made during the MDOE approach in terms of number of noses and values of roughness definition.

As mentioned before, the interchangeable noses will be characterized by different values of surface "roughness".

The nose roughness (RMS), resumed in Table 3, is defined as a variation in the height of the nose surface with respect to the nose nominal surface up to values of the order of millimetre. Moreover, the roughness distribution on the nose has to be as uniform as possible. The nose and the roughness applied on it shall also be manufactured in order to resist to both the high temperature that the nose itself will experience during the tests and the ablation due to the rust particles (about 0.01g) carried by the wind tunnel hypersonic flow.

The problem is that it is not possible to obtain a rough nose having the specified requirement by using conventional machining technique. Rapid prototyping techniques could be used, but in this case the critical items are the kind of material, the surface tolerance, and the way for defining a starting CAD reference "rough" surface for each of the roughness to be replaced. A series of study and tests has been performed by CIRA in cooperation with the CSM (Italian Study Centre for Material) in order to select the best methodology to realise the rough noses.

VII. Conclusions

The understanding of the mechanisms leading to transition and the development of reliable transition prediction methods are recognized as critical issues in aerothermodynamics..

An experimental activity was planned in CIRA in order to investigate the bluntness and the distributed roughness effects on a 3-deg half-angle sphere-cone model, taking into account Reynolds and Mach number variations. The aim of the activities is to improve the understanding of the transition mechanisms in hypersonic flow and, at the same time, to improve the effectiveness of the existing transition prediction criteria.

In the present work the design of a CIRA experiment, planned for in next months, has been illustrated.

In order to define the basic requirement definition for both the model design and for experimental test campaign a preliminary numerical CFD analysis has been performed, giving as results the preliminary model nose radius and roughness range.

Then the modern design of experiment (MDOE), a modern statistical method, first introduced at NASA Langley Research Center in 1997 to produce aerospace research results at the lowest cost consistent with a specified maximum levels of uncertainty, has been applied in the present work to develop highly efficient experiment designs yielding results to within a specified precision and, at the same time, saving resource in terms of costs (nose number minimization of test runs by optimizing the test points' position in the design space).

Finally a brief model design description has been illustrated, and an innovative and at the same time simple rough nose realization methodology definition has been investigated, being this one an essential step of the experiment design phase, in order to guarantee a more "degree of freedom" for the choices to be made during the MDOE study in terms of number of noses and values of roughness definition.

Acknowledgments

The authors wish a sincere and grateful acknowledgement to Dr. Alessio Nicolì, whose participation in the very early stage of this activity is strongly recognized, to Paolo Piscopo that made an excellent CAD design work, to Donato De Rosa that made infinite CFD analyses and to Biagio Imperatore whose experience, aided to solve all critical choices concerning the model design and the instrumentation selection to be installed on the model.

A special thank goes to Steven P. Schneider, whose kind and thorough suggestions significantly eased in some case the design of the experiments and to Dr.Franco Anzani and Dr. Maria Pia D'Ambrosio, whose precepts significantly aided to approach the MDoE philosophy.

Finally, the authors wish a sincere and grateful to Italian Study Centre for Material (CSM) and in particular to M. Tului and S. Lionetti whose cooperation has been essential for the rough nose realization technique definition.

References

[1] J.D. Anderson. Hypersonic and High Temperature Gas Dynamics. AIAA. 2000.

[2] Steven P. Schneider. Hypersonic laminar-turbulent transition on circular cones and scram-jet forebodies. Progress in Aerospace Sciences, 40(1-2):1{50, 2004.

[3] R.G. Batt & H.H. Legner: A review of roughness induced nosetip transition. AIAA Journal, Vol. 21, No 1, January 1983, pp 7-22.

[4] D.C. Reda: Corrrelation of nosetip boundary layer transition data measured in ballistics-range experiments. AIAA Journal, Vol. 19, No 3, March 1981, pp 329-339.

[5] Reda, D.C., Review and Synthesis of Roughness-Dominated Transition Correlations for Reentry applications, Journal of Spacecraft and Rockets, Vol. 39, No. 2, 2002, pp. 161-167.

[6] Friehmelt, H., Koppenwallner, G. and Müller-Eigner, R. Calibration and first results of a redesigned Ludwieg expansion tube, AIAA-paper 93-5001, AIAA, 1993

[7] Steven P. Schneider. Effects of high-speed tunnel noise on laminar-turbulent transition. Journal of Spacecraft and Rockets, 38(3):323{333, May{June 2001.
[8] I.E. Beckwith and C.G. Miller III. Aerothermo- dynamics and transition in high-speed wind tunnels at NASA Langley. Annual Review of Fluid Mechanics, 22:419{439, 1990.
[9] Stetson, Kenneth F., "On Cone Frustum Pressure Gradient Effects on Transition," AIAA Journal, Vol. 26, No. 4, April 1988, pp. 500-502.
[10] Stetson, K. F., "Nosetip Bluntness Effects on Cone Frustrum Boundary Layer Transition in Hypersonic Flow," AIAA Paper 83-1763, July 1983.
[11] D. J. Singh, A. Kumar, and S. N. Tiwari. Effect of nose bluntness on flow field over slender bodies in hypersonic flows. AIAA-89-0270, January 1989
[12] John D. Anderson. Hypersonic and High Temperature Gas Dynamics. McGraw-Hill, Inc., New York, 1989.
[13] M. S. Holden. Leading edge bluntness and boundary layer displacement effects on attached and separated laminar boundary layers in compression corner. AIAA-68-68, 1968.
[14] "Special Course On Aerothermodynamics of Hypersonic Vehicle" - AGARD AR-761
[15] Müller, L., Henckels, A., - "Visualization Of High-Speed Boundary-Layer Transition With FPA Infrared Technique" – DGLR96-B.
[16] Van Driest E.R, Blumer C., Wells, C.S., "Boundary-layer transition on blunt bodies - Effect of roughness", AIAA Journal Vol. 5(10), pp. 1913-1915, 1967
[17] [1] F. Vignau, "Etude théorique et expérimentale de la transition en écoulement bidimensionnel compressible", Thèse de Doctorat Sup'Aéro, December 1989
[18] S.A Bouslog, J.J. Bertin, S.A. Berry, J.M. Caram, "Isolated Roughness Induced Boundary Layer Transition Shuttle Orbiter Ground Tests and Flight Experience", AIAA Paper 97-0274, 35th Aerospace Science Meeting and Exhibit, Reno, 1997
[19] Potter J.L., Whitfield J.D., "Effets of slight nose bluntness and roughness on boundary-layer transition in supersonic flow", Journal of Fluid Mechanics, vol. 12(4), pp. 501-535, 1962
[20] Anderson A.D., "Passive Nosetip Technology (PANT) Program" Interim report, Volume X, Appendix A : Boundary Layer Transition on Nosetips with Rough Surfaces. SAMSO-TR-74-86, Jan. 1975
[21] Reda D.C., "Correlation of nose tip boundary-layer transition data measured in ballistics-range experiments", AIAA Paper 80-0286 and Sandia National Labs. Rep SAND-79-0649, November 1979
[22] Batt R.G., Legner H.H., "A review of roughness-induced nosetip transition", AIAA Journal, Vol. 21(1), pp 7-22, Jan. 1983
[23] D.C. Reda, "Review and Synthesis of Roughness-Dominated Transition Correlations for Reentry Applications", Journal of Spacecraft and Rockets, vol. 39(2), pp. 161-167, march 2002
[24] J.J. Bertin, T.E. Hayden, W.D. Goodrich, "Comparison of correlations of shuttle boundary-layer transition due to distributed roughness", AIAA Paper 81-417, 1981
[25] W.D. Goodrich, S.M. Derry, J.J. Bertin, "Shuttle Orbiter boundary-layer transition: A comparison of flight and wind tunnel data", AIAA Paper 83-485, 1983
[26] S.A. Berry, S.A. Bouslog, G.J. Brauckmann, J.M. Caram, "Boundary Layer Transition due to Isolated Roughness: Shuttle Results from the LaRC
[27] D.S. Liechty, S.A. Berry, B.R. Hollis, "Comparison of methods for Determining Boundary Layer Edge Conditions for Transition Correlation", AIAA Paper 2003-3590, 33rd AIAA Fluid Dynamics Conference and Exhibit, Orlando, June 2003
[28] A.H. Boudreau, "Correlation of Artificially Induced Boundary-Layer Transition Data at Hypersonic Speeds", Journal of Spacecraft and Rockets. Vol. 18, no. 2, pp. 152-156. 1981
[29] Reshotko E, Tumin A, "Role of transient growth in roughness-induced transition" AIAA Journal, vol. 42(4), Apr. 2004, pp. 766-770
[30] Rode M, DeLoach R.- "Hypersonic Wind Tunnel Calibration Using the Modern Design of Experiments" - AIAA-paper 2005-4274.
[31] Douglas C. Montgomery - "Design and Analysis of Experiments 5th edition" – John Wiley & Sons Inc.
[32] Marino, A., Imperatore, B., Ragni, A., "Streamwise porosity distribution optimization for minimising wall interference in a transonic wind tunnel", AIAA - 2009-1485